Fracture Mechanics of Concrete and Concrete Structures -
Recent Advances in Fracture Mechanics of Concrete - B. H. Oh, et al.(eds)
ⓒ 2010 Korea Concrete Institute, Seoul, ISBN 978-89-5708-180-8

A generalized discrete strong discontinuity approach

D. Dias-da-Costa
ISISE, Civil Engineering Department, University of Coimbra, Coimbra, Portugal

J. Alfaiate
IST and ICIST, Civil Engineering Department, Instituto Superior Técnico, Lisboa, Portugal

L.J. Sluys
Civil Engineering and Geosciences Department, Delft University of Technology, Delft, The Netherlands

E. Júlio
ISISE, Civil Engineering Department, University of Coimbra, Coimbra, Portugal

ABSTRACT: Several local embedded discontinuity formulations have already been developed, in which constant strain triangles and constant jumps are adopted. However, these formulations lead to jump and traction discontinuity across element boundaries and stress locking effects. Herein, a new contribution to embedded strong discontinuities is given. A generalized discrete strong discontinuity approach (GSDA) is presented, in which non-homogeneous jumps can be embedded in any type of parent finite elements. A comparison to the generalized finite element method (GFEM) is also established. With this new formulation the additional degrees of freedom are global and continuous jumps and tractions across the element boundaries are always obtained. The kinematics of the GSDA accurately reproduces both rigid-body motion and stretching induced by the opening of a discontinuity. Some simple examples are presented to illustrate the ability of this formulation in reproducing different opening modes. Structural examples, involving both mode-I and mixed-mode fracture, are also simulated and compared to experimental results.

1 INTRODUCTION

The numerical modeling of fracture behavior of quasi-brittle materials still poses important challenges. Before a *true* crack is formed, microcracking extends over a significant area ahead of the crack tip, rendering the traditional assumptions of linear elastic fracture cumbersome.

The cohesive crack model proposed by Hillerborg, Modeer et al. (1976) allowed for the simulation of discrete cracking. Initially, zero-thickness interface elements were applied. However, only after the development of finite elements with strong embedded discontinuities, a more efficient modeling of strain localization problems could be achieved. Most existing formulations (Dvorkin, Cuitiño et al. 1990, Simo & Rifai 1990, Klisinski, Runesson et al. 1991, Lofti & Shing 1995, Armero & Garikipati 1996, Larsson & Runesson 1996, Oliver 1996, Wells & Sluys 2001, Oliver, Huespe et al. 2002) take advantage of a static condensation, at element level, in order to keep the number of degrees of freedom constant. As a consequence, a discontinuous jump profile across element boundaries is obtained. Moreover, constant strain triangles (CST) enriched with constant jumps are usually applied, leading to well-known stress locking problems (Jirásek 2000).

In the embedded formulations introduced by Bolzon (2001) and Linder & Armero (2007) linear displacement jumps at the discontinuity are adopted. However, the traditional CST elements are still used in the former case, whereas a local formulation is applied for both cases. In Dias-da-Costa, Alfaiate et al. (2009), a global formulation is presented, in which a non-homogeneous jump displacement field is considered across the discontinuity. These displacement jumps are transmitted to the parent element nodes by means of a rigid body motion. As a consequence, constant shear jumps are enforced, thus neglecting the *stretching* induced by the opening of a discontinuity.

Recently, the generalized finite element method (GFEM), also known as extended finite element method (XFEM), became a powerful numerical tool available for the simulation of discontinuities (Duarte & Oden 1995, Melenk & Babuska 1996, Belytschko & Black 1999, Moës, Dolbow et al. 1999, Duarte, Babuska et al. 2000). This is a nodal enrichment technique, in which the partition of unity property of the shape functions is exploited to approximate the strong discontinuity kinematics.

In this paper, a generalized strong discontinuity approach (GSDA) is presented and compared to the GFEM method. Conversely to previous embedded formulations (Alfaiate, Simone et al. 2003, Dias-da-Costa, Alfaiate et al. 2009), all available degrees of freedom at the discontinuity are taken into account in order to capture both *rigid body motion* and *stretching*. This formulation can be applied to any parent element. Moreover, the additional degrees of freedom are global, meaning that the discontinuity jumps and tractions are kept continuous across element boundaries.

In Section 2 the problem description is presented, including the variational framework (Section 2.1), which is the same for the GSDA and the GFEM. The discretization of the variational equations is performed in Section 2.2. Some issues related to the numerical implementation are briefly reviewed in Section 3. The constitutive relation used in the computed examples is presented in Section 4. In Section 5.1 simple examples are computed in order to reveal particular aspects connected to the kinematics of both numerical techniques. Next, in Section 5.2, two structural examples are presented, one including mixed-mode fracture. Finally, in Section 6, the most relevant conclusions are presented.

2 PROBLEM DESCRIPTION

2.1 *Common framework*

In this Section the kinematics of a strong discontinuity is briefly addressed. More detail can be found elsewhere (see, for instance, Dias-da-Costa, Alfaiate et al. (2009)).

Consider an elastic domain Ω, with boundary Γ, containing a discontinuity surface Γ_d defining two subregions Ω^+ and Ω^-, according to Figure 1.

A quasi-static loading composed by body forces, $\bar{\mathbf{b}}$, and natural boundary conditions, $\bar{\mathbf{t}}$, the latter distributed on the external boundary, Γ_t, are applied to the body. The essential boundary conditions $\bar{\mathbf{u}}$ distributed on the remaining part of the boundary, Γ_u, such that $\Gamma_t \cup \Gamma_u = \Gamma$ and $\Gamma_t \cap \Gamma_u = \varnothing$. The vector $\mathbf{n}$ is orthogonal to the boundary surface, pointing outwards, whereas $\mathbf{n}^+$ is orthogonal to the internal discontinuity surface, pointing inwards Ω^+ (see Fig. 1).

The total displacement $\mathbf{u}$ is decomposed according to the following equation:

$$\mathbf{u}(\mathbf{x}) = \hat{\mathbf{u}}(\mathbf{x}) + \mathrm{H}_{\Gamma_d} \tilde{\mathbf{u}}(\mathbf{x}), \qquad (1)$$

where $\hat{\mathbf{u}}$ represents the regular displacement field and $\tilde{\mathbf{u}}$ is the enhanced displacement field. H_{Γ_d} is a function defining the jump transmission by the discontinuity. Here, the standard Heaviside function is chosen.

The strain field is defined, under small displacements hypothesis, as the symmetric part of the gradient of the displacement field:

$$\boldsymbol{\varepsilon} = \nabla^s \mathbf{u} = \underbrace{\nabla^s \hat{\mathbf{u}} + \mathrm{H}_{\Gamma_d} \nabla^s \tilde{\mathbf{u}}}_{bounded} + \underbrace{\delta_{\Gamma_d} \left([\![\mathbf{u}]\!] \otimes \mathbf{n} \right)^s}_{\text{unbounded}} \quad \text{in } \Omega, \qquad (2)$$

where $(\cdot)^s$ stands for the symmetric part of $(\cdot)$ and $\otimes$ denotes the dyadic product.

Both displacement and strain fields remain continuous in Ω^- and Ω^+, since the unbounded term in Equation (2) vanishes in $\Omega \setminus \Gamma_d = \Omega^- \cup \Omega^+$.

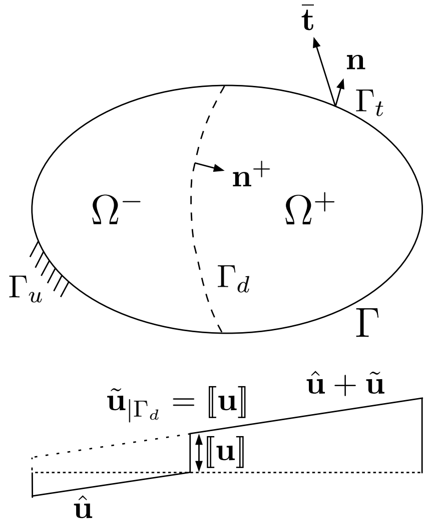

Figure 1. Domain Ω crossed by a discontinuity surface Γ_d.

Under quasi-static equilibrium conditions, the variational formulation can be cast into the following form:

$$\begin{aligned} &\int_{\Omega \setminus \Gamma_d} \left(\nabla^s \delta \hat{\mathbf{u}} \right) : \boldsymbol{\sigma}(\boldsymbol{\varepsilon}) \, d\Omega = \\ &= \int_{\Omega \setminus \Gamma_d} \delta \hat{\mathbf{u}} \cdot \bar{\mathbf{b}} \, d\Omega + \int_{\Gamma_t} \delta \hat{\mathbf{u}} \cdot \bar{\mathbf{t}} \, d\Gamma \end{aligned} \qquad (3)$$

and

$$\begin{aligned} &\int_{\Omega^+} \left(\nabla^s \delta \tilde{\mathbf{u}} \right) : \boldsymbol{\sigma}(\boldsymbol{\varepsilon}) \, d\Omega + \int_{\Gamma_d} \delta [\![\mathbf{u}]\!] \, \mathbf{t}^+ d\Gamma = \\ &= \int_{\Omega^+} \delta \tilde{\mathbf{u}} \cdot \bar{\mathbf{b}} \, d\Omega + \int_{\Gamma_t^+} \delta \tilde{\mathbf{u}} \cdot \bar{\mathbf{t}} \, d\Gamma, \end{aligned} \qquad (4)$$

where $\delta \hat{\mathbf{u}}$ and $\delta \tilde{\mathbf{u}}$ are, respectively, the regular and enhanced virtual displacements.

Both GSDA and GFEM formulations share the same variational framework defined by Equation (3) and (4). However, the GSDA remains an element enrichment technique, whereas the GFEM is a nodal enrichment technique. Therefore, discretization is addressed separately in the following subsection.

2.2 *Discretization*

In this section the discretized equations for both formulations are presented.

2.2.1 *GSDA*

The displacement field within each enriched element domain, Ω^e, can be cast in the following form:

$$\mathbf{u}^e = \mathbf{N}^e(\mathbf{x})\left[\mathbf{a}^e + \left(\mathrm{H}_{\Gamma_d}\mathbf{I} - \mathbf{H}^e_{\Gamma_d}\right)\tilde{\mathbf{a}}^e\right] \text{ if } \mathbf{x} \in \Omega^e \setminus \Gamma_d, \quad (5)$$

$$[\![\mathbf{u}]\!]^e = \mathbf{N}^e_w\left[s(\mathbf{x})\right]\mathbf{w}^e \text{ at } \Gamma^e_d, \quad (6)$$

where $\mathbf{N}^e$ contains the element shape functions, $\mathbf{a}^e$ are the total nodal displacements, $\tilde{\mathbf{a}}^e$ are the enhanced nodal displacements, $\mathbf{I}$ is a $(2n \times 2n)$ identity matrix and $\mathbf{H}^e_{\Gamma_d}$ is a $(2n \times 2n)$ diagonal matrix composed by successively evaluating the Heaviside function at each of the $2n$ degrees of freedom of the finite element. $\mathbf{N}^e_w$ is a $(d \times n_w)$, ($d = 2$ in 2D and $d = 3$ in 3D), matrix containing the shape functions used to approximate the jumps $[\![\mathbf{u}]\!]^e$, which are reflected by degrees of freedom $\mathbf{w}^e$ measured at the n_w additional nodes, and $s(\mathbf{x})$ is the coordinate along the discontinuity defined by Figure 2. n_w is related to the degree used to approximate the jumps: two additional nodes along Γ_d are used for a linear function (nodes i and j from Figure 2).

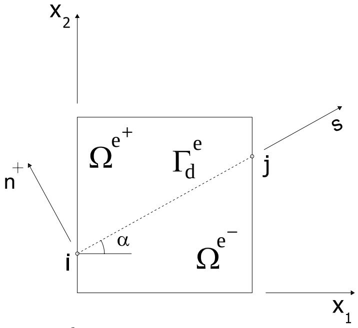

Figure 2. Domain Ω^e crossed by a discontinuity surface Γ^e_d.

The enhanced nodal displacements are obtained from:

$$\tilde{\mathbf{a}}^e = \mathbf{M}^{ek}_w\mathbf{w}^e, \quad (7)$$

where $\mathbf{M}^{ek}_w$ is a matrix transmitting the jumps to the nodes of the enriched finite element. This matrix is formed by stacking, in rows, a matrix $\mathbf{M}^e_w$ evaluated at each node of the element. $\mathbf{M}^e_w$ is decomposed into two matrices containing: (i) a linear shear slide, $\mathbf{M}_{\mathbf{s}_\mathbf{w}}{}^e$; and (2) a rigid body rotation and translation normal to the discontinuity, $\mathbf{M}_{\mathbf{n}_\mathbf{w}}{}^e$:

$$\mathbf{M}^e_w = \mathbf{M}_{\mathbf{s}_\mathbf{w}}{}^e + \mathbf{M}_{\mathbf{n}_\mathbf{w}}{}^e, \quad (8)$$

with

$$\mathbf{M}_{\mathbf{s}_\mathbf{w}}{}^e = \frac{1}{2}\begin{bmatrix} \left(1 - s^e_n\right)\left(1 + c2a\right) & \left(1 - s^e_n\right)s2a & s^e_n\left(1 + c2a\right) & s^e_n\left(s2a\right) \\ \left(1 - s^e_n\right)s2a & \left(1 - s^e_n\right)\left(1 - c2a\right) & s^e_n\left(s2a\right) & s^e_n\left(1 - c2a\right) \end{bmatrix}, \quad (9)$$

$$\mathbf{M}_{\mathbf{n}_\mathbf{w}}{}^e = \begin{bmatrix} \frac{1 - c2a}{2} - \frac{\left(x_2 - x^i_2\right)sa}{l^e_d} & -\frac{s2a}{2} + \frac{\left(x_2 - x^i_2\right)ca}{l^e_d} & \frac{\left(x_2 - x^i_2\right)sa}{l^e_d} & -\frac{\left(x_2 - x^i_2\right)ca}{l^e_d} \\ -\frac{s2a}{2} + \frac{\left(x_1 - x^i_1\right)sa}{l^e_d} & \frac{1 + c2a}{2} - \frac{\left(x_1 - x^i_1\right)ca}{l^e_d} & -\frac{\left(x_1 - x^i_1\right)sa}{l^e_d} & \frac{\left(x_1 - x^i_1\right)ca}{l^e_d} \end{bmatrix}. \quad (10)$$

In Equation (9) and (10), $sa = \sin(\alpha)$, $ca = \cos(\alpha)$, $s2a = \sin(2\alpha)$, $c2a = \cos(2\alpha)$, and:

$$s^e_n = \frac{s(\mathbf{x}_i)}{l^e_d} = (x_1 - x^i_1)\frac{\cos(\alpha)}{l^e_d} + (x_2 - x^i_2)\frac{\sin(\alpha)}{l^e_d}, \quad (11)$$

$\mathbf{x} = \left(\mathbf{x}_1, \mathbf{x}_2\right)$ is the global position of any material point inside the finite element, $\mathbf{x}^i = \left(\mathbf{x}^i_1, \mathbf{x}^i_2\right)$ is the global position of the tip i, l^e_d is the length of the discontinuity Γ^e_d measured along the local frame $\mathbf{s}$ and α is the discontinuity angle (see Fig. 2).

The strain field is approximated using the standard strain-displacement matrix, $\mathbf{B}^e$:

$$\boldsymbol{\varepsilon}^e = \mathbf{B}^e(\mathbf{x})\left[\mathbf{a}^e + \left(\mathrm{H}_{\Gamma_d}\mathbf{I} - \mathbf{H}^e_{\Gamma_d}\right)\tilde{\mathbf{a}}^e\right]. \quad (12)$$

The incremental stress field and incremental traction at the discontinuity are given by:

$$d\boldsymbol{\sigma}^e = \mathbf{D}^e\mathbf{B}^e[d\mathbf{a}^e + \left(\mathrm{H}_{\Gamma_d}\mathbf{I} - \mathbf{H}^e_{\Gamma_d}\right)d\tilde{\mathbf{a}}^e], \quad (13)$$

$$d\mathbf{t}^e = \mathbf{T}^e d[\![\mathbf{u}]\!]^e = \mathbf{T}^e\mathbf{N}^e_w d\mathbf{w}^e \text{ at } \Gamma^e_d, \quad (14)$$

where $\mathbf{T}^e$ is the discontinuity constitutive matrix.

Taking into account Equation (5) into (14), the descritization of Equation (3) and (4) leads to the following system of equations:

$$\mathbf{K}^e_{aa}d\mathbf{a}^e + \mathbf{K}^e_{aw}d\mathbf{w}^e = d\hat{\mathbf{f}}^e, \quad (15)$$

$$\mathbf{K}^e_{wa}d\mathbf{a}^e + \left(\mathbf{K}^e_{ww} + \mathbf{K}^e_d\right)d\mathbf{w}^e = d\mathbf{f}^e_w, \quad (16)$$

with $\mathbf{K}^e_{aa} = \int_{\Omega^e \setminus \Gamma^e_d}\mathbf{B}^{eT}\mathbf{D}^e\mathbf{B}^e d\Omega$, $\mathbf{K}^e_{aw} = \int_{\Omega^e \setminus \Gamma^e_d}\mathbf{B}^{eT}\mathbf{D}^e\mathbf{B}^e_w d\Omega^e$, $\mathbf{K}^e_{wa} = \int_{\Omega^e \setminus \Gamma^e_d}\mathbf{B}^{eT}_w\mathbf{D}^e\mathbf{B}^e d\Omega^e$, $\mathbf{K}^e_{ww} = \int_{\Omega^e \setminus \Gamma^e_d}\mathbf{B}^{eT}_w\mathbf{D}^e\mathbf{B}^e_w d\Omega^e$, $\mathbf{K}^e_d = \int_{\Gamma^e_d}\mathbf{N}^{e\,T}_w\mathbf{T}^e\mathbf{N}^e_w d\Gamma$, $\mathbf{B}^e_w = \mathbf{B}^e\mathrm{M}^{ek}_w$, $\mathrm{M}^{ek}_w = \left(\mathrm{H}_{\Gamma_d}\mathbf{I} - \mathbf{H}^e_{\Gamma_d}\right)\mathbf{M}^{ek}_w$, $d\hat{\mathbf{f}}^e = \int_{\Omega^e \setminus \Gamma^e_d}\mathbf{N}^{eT}\bar{\mathbf{b}}^e d\Omega + \int_{\Gamma^e_t}\mathbf{N}^{eT}\bar{\mathbf{t}}^e d\Gamma$ and $d\mathbf{f}^e_w = \int_{\Omega^e}\mathrm{M}^{ekT}_w\mathbf{N}^{eT}\bar{\mathbf{b}}^e d\Omega + \int_{\Gamma^e_t}\mathrm{M}^{ekT}_w\mathbf{N}^{eT}\bar{\mathbf{t}}^e d\Gamma$.

The additional degrees of freedom are considered global; as a consequence, both jump and traction continuity are obtained across elements. Traction continuity is enforced in the weak sense. Therefore, the symmetry is kept if the constitutive material law is symmetric.

2.2.2 *GFEM*

The derivation of the discretized equations for the GFEM is well known and therefore omitted. The corresponding system of equations is:

$$\mathbf{K}^e_{\hat{a}\hat{a}} d\hat{\mathbf{a}}^e + \mathbf{K}^e_{\hat{a}\tilde{a}} d\tilde{\mathbf{a}}^e = d\hat{\mathbf{f}}^e, \quad (17)$$

$$\mathbf{K}^e_{\tilde{a}\hat{a}} d\hat{\mathbf{a}}^e + \left(\mathbf{K}^e_{\tilde{a}\tilde{a}} + \mathbf{K}^e_d\right) d\tilde{\mathbf{a}}^e = d\tilde{\mathbf{f}}^e, \quad (18)$$

where $\mathbf{K}^e_{\hat{a}\hat{a}} = \int_{\Omega^e \setminus \Gamma^e_d} \mathbf{B}^{eT}\mathbf{D}^e\mathbf{B}^e d\Omega$, $\mathbf{K}^e_{\tilde{a}\tilde{a}} = \int_{\Omega^{e+}} \mathbf{B}^{eT}\mathbf{D}^e\mathbf{B}^e d\Omega^e$, $\mathbf{K}^e_{\hat{a}\tilde{a}} = \mathbf{K}^e_{\tilde{a}\hat{a}} = \mathbf{K}^{eT}_{\tilde{a}\tilde{a}}$, $\mathbf{K}^e_d = \int_{\Gamma^e_d} \mathbf{N}^{eT}\mathbf{T}^e\mathbf{N}^e d\Gamma$, $d\hat{\mathbf{f}}^e = \int_{\Omega^e} \mathbf{N}^{eT} d\bar{\mathbf{b}}^e d\Omega + \int_{\Gamma^e_t} \mathbf{N}^{eT} d\bar{\mathbf{t}}^e d\Gamma$, $d\tilde{\mathbf{f}}^e = \int_{\Omega^{e+}} \mathbf{N}^{eT} d\bar{\mathbf{b}}^e d\Omega + \int_{\Gamma^{e+}_t} \mathbf{N}^{eT} d\bar{\mathbf{t}}^e d\Gamma$

3 NUMERICAL IMPLEMENTATION

3.1 *Crack propagation technique*

A discontinuity is considered straight, always crossing a complete parent element. Under crack propagation, additional degrees of freedom must be added to the GSDA and the GFEM. Only one discontinuity is allowed at each parent element, although generalizations can be made for more than one (Daux, Moës et al. (2000); Dias-da-Costa, Alfaiate et al. (2009)).

The direction of crack propagation is evaluated applying Rankine criterion to an averaged stress tensor. A Gaussian weight function, presented in Wells & Sluys (2001) is used. This function depends on the distance between integration point and discontinuity tip and also on a significant distance around the tip, designated *interaction radius*. Different suggestions for the value for the radius of influence can be found (Wells & Sluys (2001); Simone (2003)). Here the value is defined as circa 1% of Hillerborg's characteristic length, $l_{ch} = G_F E / f_t^2$.

The stress field measured in the bulk is not locally in equilibrium with the traction field measured in the discontinuity. This is a direct consequence of the weak traction continuity condition adopted in Equation (4). Consequently, at crack initiation, in order to prevent the traction field at the tip to lie outside the limit surface, a conservative procedure is adopted: the discontinuities are introduced in an earlier stage, in which the stress field in the bulk lies inside the Rankine limit surface.

3.2 *Numerical integration*

In order to solve for the equilibrium equation presented in Section 2.2, several numerical integrations need to be performed.

Regarding the integration of the discontinuity stiffness, $\mathbf{K}^e_d$, a two point Newton-Cotes/Lobatto scheme is applied in the GSDA, in order to avoid spurious oscillations (Dias-da-Costa, Alfaiate et al. (2009)). Consequently, these integration points coincide with the additional nodes located at the intersection of the discontinuity with the element edges (Fig. 2).

With respect to the bulk stiffness, the subregion Ω^{e+} is divided in triangles defined by the centroid of Ω^{e+} and each edge surrounding Ω^{e+}. These triangular areas are afterwards integrated by a midpoint rule with three points. All remaining integrals, spanning over Ω^e, are computed by the usual Gaussian rule.

4 CONSTITUTIVE RELATIONS

In all examples presented in the following sections, the bulk is considered linear elastic. In the following, a brief review of the discontinuity traction-separation law is presented. A more comprehensive description, regarding plastic and damage models, can be found in Alfaiate, Wells et al. (2002); Dias-da-Costa, Alfaiate et al. (2009).

4.1 *Isotropic damage law*

The constitutive law for the isotropic damage law is given by:

$$\mathbf{t} = (1-d)\mathbf{T}_{el}\mathbf{w}, \quad (19)$$

where d is a scalar damage variable such that $0 \le d \le 1$ and $\mathbf{T}_{el}$ is the initial elastic constitutive tensor.

The evolution of damage is written as:

$$d = d(\kappa) = 1 - \frac{\kappa_0}{\kappa}\exp\left(-\frac{f_{t0}}{G_F}(\kappa - \kappa_0)\right), \quad (20)$$

where f_{t0} is the initial tensile strength, G_F is the fracture energy, and κ is a scalar equivalent jump damage parameter depending on the maximum ever reached positive normal jump component, $< w_n >^+$, and shear jump component, $| w_s |$:

$$\kappa = \kappa(\mathbf{w}) = \max < w_n >^+ + \beta \max | w_s |. \qquad (21)$$

β, which is always non-negative, defines the contribution of the shear jump component to the equivalent jump parameter. At the onset of localization, $w_s = 0$ and $t_s = 0$, whereas $w_n = \kappa_0$ and $t_n = f_{t0}$.

A load function, in the displacement jump space, is defined as:

$$f = < w_n >^+ + \beta | w_s | - \kappa. \qquad (22)$$

The incremental constitutive relation can be derived from differentiation of Eq. (19):

$$\dot{\mathbf{t}} = (1-d)\mathbf{T}^{el}\dot{\mathbf{w}} - \dot{d}\mathbf{T}^{el}\mathbf{w} = (1-d)\mathbf{T}^{el}\dot{\mathbf{w}} - \dot{d}\mathbf{t}^{el}, \qquad (23)$$

where $\mathbf{t}^{el}$ is the elastic traction vector and:

$$\dot{d} = \frac{\partial d}{\partial \kappa}\frac{\partial \kappa}{\partial \mathbf{w}}\dot{\mathbf{w}}. \qquad (24)$$

Finally, Eq. (23) can be cast into the following form:

$$\dot{\mathbf{t}} = \left[(1-d)\mathbf{T}^{el} - \frac{\partial d}{\partial \kappa}\, \mathbf{t}^{el} \otimes \frac{\partial \kappa}{\partial \mathbf{w}} \right] \dot{\mathbf{w}}. \qquad (25)$$

If unloading takes place, the rate of damage is zero and the following relation is recovered:

$$\dot{\mathbf{t}} = (1-d)\mathbf{T}^{el}\dot{\mathbf{w}}. \qquad (26)$$

5 NUMERICAL EXAMPLES

Some examples are computed to compare the performance of the GSDA and the GFEM. First, one element examples are presented for two different situations: i) a discontinuity significantly softer than the bulk; and ii) vice-versa. Next, an example with stretching is also shown. Finally, two structural examples are computed, the last of them including mixed-mode fracture. Plane stress state is assumed.

5.1 *Simple examples*

5.1.1 *Soft discontinuity with rigid bulk vs. rigid discontinuity with soft bulk*

A horizontal discontinuity is placed at half the height of the parent element $(1 \times 1 \times 1\ \text{mm}^3)$. A unit load is either vertically or horizontally applied at the top left node, to induce mode-I and mode-II crack opening, respectively. A linear elastic constitutive law is adopted for the discontinuity:

$$\mathbf{T}^e = \begin{bmatrix} k_s & 0 \\ 0 & k_n \end{bmatrix}, \qquad (27)$$

Two situations are simulated: i) a soft discontinuity ($k_n = 1$ N/mm^3 and $k_s = 10^5$ N/mm^3, for mode-I; $k_n = 10^5$ N/mm^3 and $k_s = 1$ N/mm^3, for mode-II) with stiffer bulk ($E = 10^3$ MPa; $\nu = 0$); and ii) a stiffer discontinuity ($k_n = 10^3$ N/mm^3 and $k_s = 10^5$ N/mm^3, for mode-I; $k_n = 10^5$ N/mm^3 and $k_s = 10^3$ N/mm^3, for mode-II) with a softer bulk ($E = 1$ MPa; $\nu = 0$).

The deformed meshes are shown in Figure 3 and Figure 4. For the discontinuity much softer than the bulk, the results from both formulations are the same; however, for the soft bulk the GFEM gives rise to a more deformed element due to a better refinement of the bulk. This is due to the fact that, in the GSDA, the enrichment concerns *exclusively* the discontinuity.

5.1.2 *Stretching opening mode*

In this example, a finite element $(2 \times 1 \times 1\ \text{mm}^3)$ with a horizontal discontinuity placed at half of the height of the parent element is loaded with two opposite horizontal loads, $P = 13.49$ N, at both top nodes. The following constitutive parameters are applied: $E = 30$ MPa; $\nu = 0$; and shear stiffness $k_s = 10$ N/mm^3.

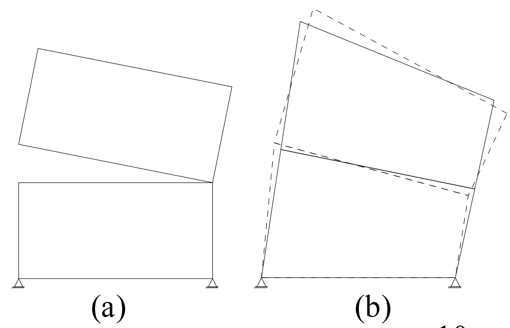

Figure 3. Mode-I deformed mesh (reduced $10\times$) for the GSDA (continuous) and the GFEM (dashed): (a) soft discontinuity; (b) soft bulk.

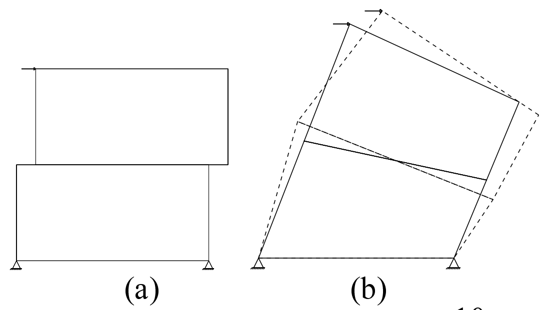

Figure 4. Mode-II deformed mesh (reduced $10\times$) for the GSDA (continuous) and the GFEM (dashed): (a) soft discontinuity; (b) soft bulk.

The overall displacement obtained with the GSDA is 15% smaller than with the GFEM – see Figure 5(a). This difference is again caused due to the smaller degree of discretization of the bulk obtained with the GSDA. For instance, for the more refined mesh represented in Figure 5(b), both formulations give rise to practically coincident results.

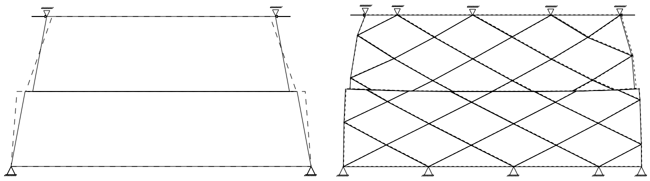

(a) (b)

Figure 5. Deformed mesh (reduced $10\times$) for the GSDA (continuous) and the GFEM (dashed): (a) one finite element; (b) distorted non-symmetric mesh.

5.2 *Structural examples*

5.2.1 *Prenotched gravity dam model*

The first structural example concerns an experimental test performed by Barpi & Valente (2000) (see Fig. 6).

Loading is performed in two stages: first deadweight is applied; afterwards, the water pressure in front of the dam is gradually increased. The arc-length method is used to enforce a monotonic increase of the relative crack mouth opening displacement (CMOD).

The material parameters of the bulk are the following: dead-weight $\rho = 2400\ \text{kg/m}^3$; Young's modulus $E = 35.7\ \text{GPa}$; Poisson's ratio $\nu = 0.1$; tensile strength $f_t = 3.6\ \text{MPa}$; and fracture energy $G_F = 0.184\ \text{N/mm}$. A discontinuity is supposed to open in mode-I of fracture, following an exponential decaying law. A gradual decrease of the elastic shear stiffness with increasing crack opening is enforced.

The mesh is composed of 1848 bilinear finite elements, with a refinement near the notch in order to better evaluate the direction of crack propagation (see Fig. 6).

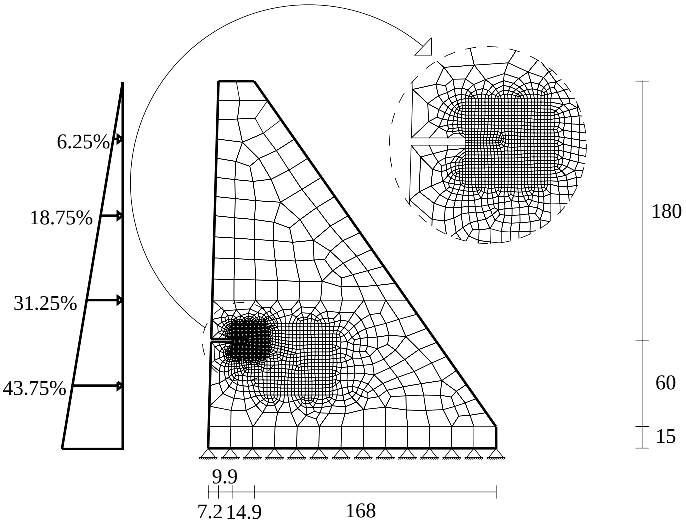

Figure 6. Prenotched gravity dam model: structural scheme (thickness 30 cm), including loading, boundary conditions and adopted mesh (all dimensions in cm).

Results are represented in Figure 7 to Figure 9. A major conclusion can be immediately drawn: both GSDA and GFEM give similar results. Furthermore, regarding the load vs. CMOD curves (Fig. 7), the numerical model appears to be steeper than the experimental curve. This is related to the mode-I constitutive relation adopted for the discontinuity. Conversely to the numerical simulation from Barpi & Valente (2000), the initial elastic stiffness is accurately simulated. Moreover, the obtained crack path, represented in Figure 8, closely follows the experimental envelope. Some differences between formulations appear only in the later stages of propagation, where the coarser mesh is clearly insufficient to evaluate the direction of crack propagation.

The deformed mesh obtained with both formulations is represented in Figure 9, when the CMOD is $0.35\ \text{mm}$.

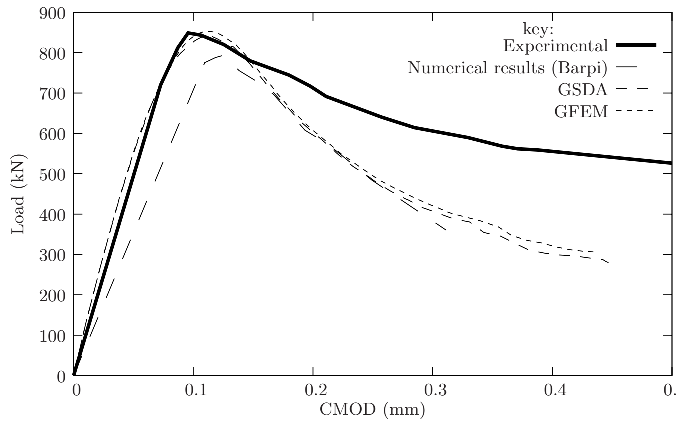

Figure 7. Prenotched gravity dam model: load vs. CMOD.

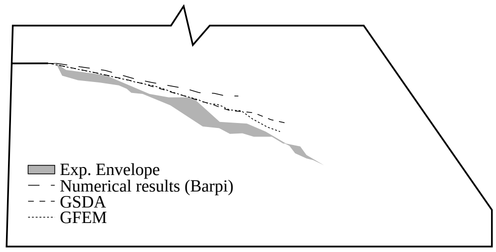

Figure 8. Prenotched gravity dam model: crack path.

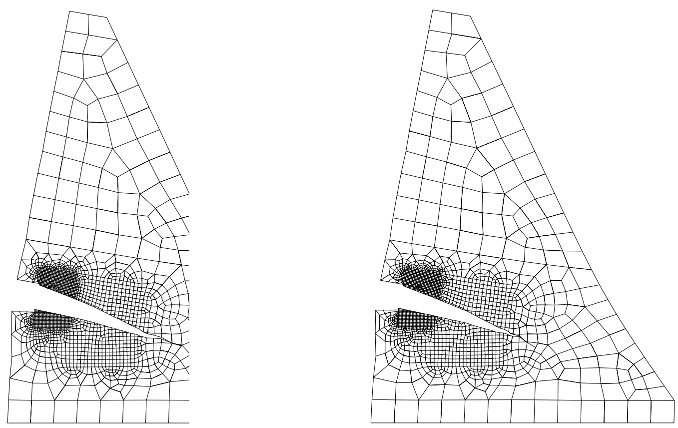

(a) (b)

Figure 9. Prenotched gravity dam model: deformed mesh (magnified $500\times$) when CMOD is 0.35 mm for: (a) GSDA; and (b) GFEM.

5.2.2 *Four-point shear test*

A mixed-mode loading benchmark, experimentally tested by Arrea & Ingraffea (1982), is numerically simulated. The details regarding the specimen geometry, mixed-mode loading and boundary conditions are represented in Figure 10.

The material properties adopted by different authors present significant differences, especially concerning the cohesive fracture properties which were not experimentally assessed (Arrea & Ingraffea (1982); Cendón, Gálvez et al. (2000)). The following constitutive parameters are adopted: Young's modulus $E = 24.8$ GPa; Poisson's ratio $\nu = 0.18$; tensile strength $f_t = 3.8$ MPa; and fracture energy $G_F = 0.125$ N/mm. The isotropic damage law presented in Section 4.1 is applied with $\beta = 0.7$ to describe the mixed-mode behavior of the discontinuity just after being inserted.

The mesh is composed of 1236 bilinear finite elements (see Fig. 10).

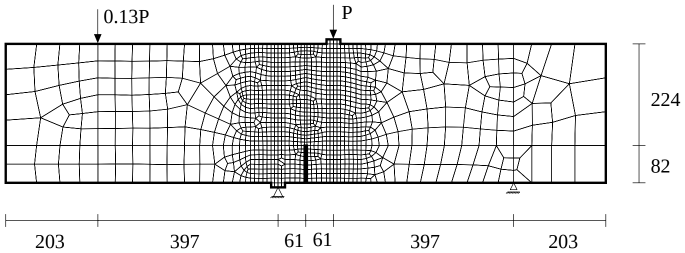

Figure 10. Four-point shear test: structural scheme (thickness 152 mm), including loading, boundary conditions and adopted mesh (all dimensions in mm).

The arc-length method is used to enforce a monotonic increase of the relative crack mouth sliding displacement (CMSD).

The numerical results are represented in Figure 11 to Figure 13. Again both GSDA and GFEM present similar results concerning both loading vs. CMSD curves and crack path. The obtained load vs. CMOD curves (Fig. 11) are within the experimental envelope. In relation to the crack path (Fig. 12) the numerical results inflect slightly inwards with respect to the experimental envelope.

The deformed mesh is represented in Figure 13, when the CMSD is 0.08 mm with the corresponding principal stress map.

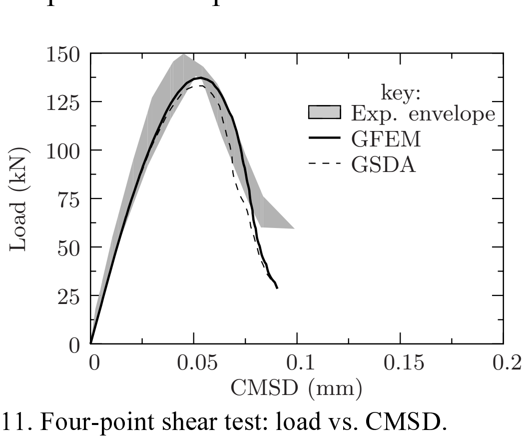

Figure 11. Four-point shear test: load vs. CMSD.

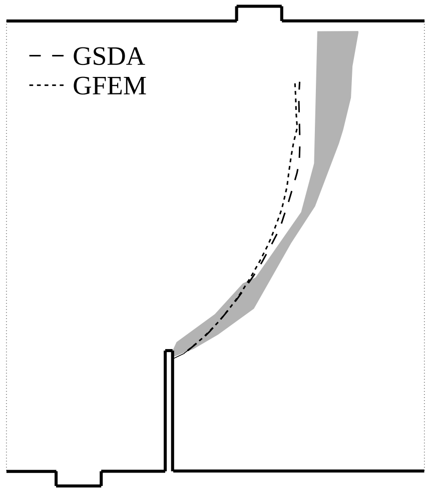

Figure 12. Four-point shear test: crack path.

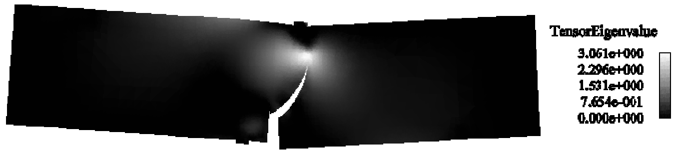

Figure 13. Four-point shear test: maximum principle stress map in the deformed mesh (magnified $200\times$) when CMSD is 0.08 mm for GFEM.

6 CONCLUSIONS

In this paper, a generalized strong embedded discontinuity approach, GSDA, has been presented. This is a new embedded discontinuity technique in which the additional global degrees of freedom are located at the discontinuity, which is explicitly inserted into the parent element. For problems in which boundary conditions must be explicitly introduced at the discontinuity, such as moisture, temperature or crack repairing with epoxy, benefit can be taken from such implementation. These additional degrees of freedom are capable of describing both the rigid body motion and the stretching induced by a discontinuity opening. Additionally, both traction and jump continuity across element boundaries are obtained.

Comparison with the GFEM method was established. Although different in nature, they have a common variational framework. The GFEM is based on the partition of unity concept, meaning that the additional degrees of freedom are introduced at the nodes to reproduce the kinematics of complex continua; as a consequence, the GFEM provides an inherent better refinement of the bulk, which could be observed using simple examples. Nevertheless, for quasi-brittle materials, in which case the discontinuity is considerably softer than the bulk, this better bulk refinement is found to be unimportant. Indeed, it was found that both methods produce identical results in the analysis of two different structural examples: i) a prenotched gravity dam under mode-I fracture and ii) a four point bending beam subjected to mixed-mode fracture.

ACKNOWLEDGMENTS

The authors acknowledge the financial support of the Portuguese Science and Technology Foundation (FCT), Ph.D. Grant number SFRH/BD/40349/2007.

REFERENCES

Alfaiate, J., A. Simone, et al. 2003. Non-homogeneous displacement jumps in strong embedded discontinuities. *International Journal of Solids and Structures* 40(21): 5799-5817.

Alfaiate, J., G. N. Wells, et al. 2002. On the use of embedded discontinuity elements with crack path continuity for mode-I and mixed-mode fracture. *Engineering Fracture Mechanics* 69(6): 661-686.

Arrea, M. & A. Ingraffea 1982. *Mixed mode crack propagation in mortar and concrete*. Report 81-13, Department of Structural Engineering, Cornell University.

Barpi, F. & S. Valente 2000. Numerical simulation of prenotched gravity dam models. *Journal of Engineering Mechanics* 126(6): 611-619.

Belytschko, T. & T. Black 1999. Elastic crack growth in finite elements with minimal remeshing. *International Journal for Numerical Methods In Engineering* 45(5): 601-620.

Bolzon, G. 2001. Formulation of a triangular finite element with an embedded interface via isoparametric mapping. *Computational Mechanics* 27(6): 463-473.

Cendón, D. A., J. C. Gálvez, et al. 2000. Modelling the fracture of concrete under mixed loading. *International Journal of Fracture* 103(3): 293-310.

Daux, C., N. Moës, et al. 2000. Arbitrary branched and intersecting cracks with the extended finite element method. *International Journal for Numerical Methods In Engineering* 48(12): 1741-1760.

Dias-da-Costa, D., J. Alfaiate, et al. 2009. A discrete strong discontinuity approach. *Engineering Fracture Mechanics* 76(9): 1176-1201.

Duarte, C. A. M., I. Babuska, et al. 2000. Generalized finite element methods for three-dimensional structural mechanics problems. *Computers & Structures* 77(2): 215-232.

Duarte, C. A. M. & J. T. Oden 1995. *H-p clouds - an h-p meshless method*.

Hillerborg, A., M. Modeer, et al. 1976. Analysis of crack formation and crack growth in concrete by means of fracture mechanics and finite elements. *Cement and Concrete Research* 6(6): 773-781.

Jirásek, M. 2000. Comparative study on finite elements with embedded discontinuities. *Computer Methods in Applied Mechanics and Engineering* 188(1-3): 307-330.

Linder, C. & F. Armero 2007. Finite elements with embedded strong discontinuities for the modeling of failure in solids. *International Journal for Numerical Methods In Engineering* 72(12): 1391-1433.

Melenk, J. M. & I. Babuska 1996. The partition of unity finite element method: Basic theory and applications. *Computer Methods in Applied Mechanics and Engineering* 139(1-4): 289-314.

Moës, N., J. Dolbow, et al. 1999. A finite element method for crack growth without remeshing. *International Journal for Numerical Methods in Engineering* 46(1): 131-150.

Simone, A. 2003. *Continuous-Discontinuous Modelling of Failure*. Ph.D., Civil Engineering and Geosciences, Delft University of Technology.

Wells, G. N. & L. J. Sluys 2001. A new method for modelling cohesive cracks using finite elements. *International Journal for Numerical Methods in Engineering* 50(12): 2667-2682.